Proceedings World Geothermal Congress 2020+1
Reykjavik, Iceland, April - October 2021

Interpreting the Structural of the Montserrat Geothermal System Using Machine Learning

Racine A. Basant and Graham A. Ryan

The Seismic Research Centre, University of the West Indies, St. Augustine Campus, Trinidad and Tobago.

racinebasant@gmail.com

graham.ryan.uwisrc@gmail.com

Keywords: Geophysics, fuzzy c means, cluster analysis, geothermal system, hydrothermal alteration

ABSTRACT

Developing an understanding of a geothermal system with the use of more than one geophysical dataset can help de-risk drilling prospects and help with reservoir management. This research aims to constrain the structure of the Montserrat Geothermal system (MGS) located in the western part of Montserrat, an island in the Eastern Caribbean. This study utilizes existing data obtained from three separate geophysical surveys: a magnetotellurics survey, a high-resolution seismic tomography survey and a gravity survey, to jointly interpret the structural features within the MGS. Inverse modelling of the geophysical datasets produces three dimensional subsurface models of resistivity, seismic velocity and density. These physical property estimates can then be used to help determine the spatial distribution of subsurface materials in the reservoir such as clay, unaltered rock and fluid saturated reservoir rocks. To jointly interpret the datasets, a machine learning application, the Fuzzy c- means clustering algorithm (FCM), was used in this study. The FCM method uses a distance measure and a membership function to cluster the multiparameter geophysical dataset (each point in the dataset is associated with a density contrasts, resistivity and velocity perturbation value). Utilizing two validity indices, four clusters were determined as the optimal number of clusters within the multiparameter geophysical dataset. Each cluster was interpreted based on the variations in each geophysical property. Cluster 1, 2 and 3 were interpreted as the unaltered region, clay cap and geothermal reservoir of the MGS respectively. While further investigation is needed, cluster 4 was interpreted as an intrusion possibly associated with the extinct volcanic center, Centre Hills. The advantage of the cluster analysis is that each structure is now assigned more than one geophysical parameter that can be used to refine previous calculations on petrophysical parameters, such as saturation, permeability and porosity.

1. INTRODUCTION

Montserrat is a volcanic island located in the northern section of the Lesser Antilles arc. The island is made up of four different volcanic centers (Figure 1) of overlapping activity: Silver Hills (2.17 – 1.03 Ma), Centre Hills (1.14 – 0.38 Ma), Soufrière Hills (0.45 Ma to present) and South Soufrière Hills (0.13 Ma) (Hatter, 2018).

Figure 1: Geological map of Montserrat highlighting the four volcanic centers. The area outlined in black represents the location of the Montserrat Geothermal Project area (MGPA): St. Georges Hill (SGH)- Garibaldi Hill (GH) -Richmond Hill (RH) region (Source: UWI Seismic Research Centre)

Phreatic explosions from Soufrière Hills in 1995 not only destroyed the island's capital but also caused severe economic instability. To help rebuild the nation, one of the main aims has been focused on providing clean, reliable and low-cost sustainable energy. As such, focus has been placed on developing geothermal energy on the island. A geothermal exploration program conducted in 2009 (EGS, 2010) identified the potential geothermal system within the St. Georges Hill and Garibaldi Hill region (outlined as the

Montserrat Geothermal Project area in the black box in Figure 1). Utilizing the exploration data along with a joint interpretation study (Ryan et al., 2013), two successful geothermal wells were drilled in St. Georges Hill. Both wells measured flow rates of up to 22 kg/s and 12 kg/s and temperatures of up to 230 °C and 265 °C for the two wells MON-1 and MON-2 respectively (Brophy et al., 2014)). Thus far, two joint interpretation studies, utilized resistivity data obtained from a magnetotellurics survey (Ryan et al.,2009), velocity perturbation data from a high resolution seismic tomography survey (Shalev et al.,2010) and earthquake hypocenter data (Ryan et al., 2013, Ryan and Shalev., 2014) to confirm that a geothermal system existed in the SGH-GH region and ultimately to help delineate optimum drilling targets by calculating variations in physical properties such as temperature and permeability (geophysical – physical parameters variation). While these studies have utilized only the spatial correlations amongst the geophysical datasets, we propose to improve on these studies by constraining each structural feature of the geothermal system, with the use of three independent geophysical datasets: a density contrasts (Hautmann et al., 2013), resistivity (Ryan et al., 2009) and velocity perturbation (Shalev et al., 2010). Several studies have shown that the use of more than one property can be used to develop constrained interpretations of the structural features and reduce the limitations that are associated with geophysical inversions (De Stefano et al., 2011; Gallardo and Meju, 2004; Garcia et al., 2017; Lelievre et al., 2012; Paasche et al., 2007; Paasche et al., 2010; Sun and Li, 2012). We also aim to utilize a more robust technique for grouping these datasets. Recently, machine learning techniques (both supervised and unsupervised) have been utilized to group or cluster geophysical datasets (Lelievre et al., 2012; Paasche et al., 2007; Paasche et al., 2010; Sun and Li, 2012; Sun and Li, 2016). One main advantage of clustering techniques is that they are useful in situations where little prior knowledge exists (Paasche et al., 2007). One method, the fuzzy c-means (FCM) (Bezdek, 1984) uses a membership function which tells the degree to which a datapoints belongs to a cluster. The FCM also allows for one datapoint to belong to more than one cluster unlike hard clustering techniques (k-means) which associates each datapoint to only one cluster. For this study, we implement the FCM technique for the joint interpretation of the three geophysical datasets mentioned earlier.

2. METHOD

2.1 Fuzzy c means (FCM)

The Fuzzy c means clustering technique divides an input dataset X into *c* fuzzy clusters (Bezdek, 1984). It is an iterative technique which acts to minimize the objective function or the distance between the ith cluster center and each datapoint with the use of a membership matrix. Each datapoint is assigned a membership value which ranges between 0 and 1 and expresses the degree of similarity to each cluster. 0 represents no similarities and 1 represents high similarities. The advantages of this method include its ability to classify unlabelled data and allows all datapoints within a dataset to belong partially to several clusters (Bezdek, 1984). To classify the various clusters within the dataset, the FCM method utilizes an objective function (equation 1) which evaluates the distance between the ith cluster centre (v_i) and the kth datapoint (x_k).

$$J_m(U, v) = \sum_{k=1}^{N} \sum_{i=1}^{c} (u_{ik})^m \; \| x_k - v_i \|^2 \quad (1)$$

where:

$X = \{x_1, x_2 \ldots .. x_k\}$ = data

c = number of clusters in X; 2 < c < n,

m = weighting exponent; 1 ∼< m < ∞

U = [uij] i=1…c, j=1…n = fuzzy c-partition of X

$v_i = (v_1, v_2 \ldots . v_i)$ = vectors of centers

u_{ik} = degree of membership of xi in the jth cluster between 0 and 1

$d_{ik} = \| x_k - v_i \|$ = objective function

2.2 Validity Indices

The partitioning coefficient and partitioning entropy can be used as validity indices which help evaluate the optimum number of clusters to classify the data into (Bezdek, 1981; Bezdek, 1984). The partitioning coefficient, F, evaluates the magnitude of the membership matrix (equation 3). A high value for the normalized partitioning coefficient is obtained when there is little overlap between clusters (membership values close to 1 represent points that display the highest similarity and 0 being little to no similarity). The partitioning entropy, H, is a measure of the degree of disorder or randomness in the system (equation 2). Hence, a high entropy implies a high disorder within a group of datapoints while a low entropy implies the reverse. In the case of clustering, well sorted clusters will display low entropy values. In FCM, When the data set is optimally clustered entropy is minimized and partitioning coefficient is maximized.

$$H(U, c) = \frac{1}{n} \sum_{j=1}^{n} \sum_{i=1}^{c} \left| u_{ij} ln u_{ij} \right| \quad (2)$$

$$F(U, c) = \frac{1}{n} \sum_{j=1}^{n} \sum_{i=1}^{c} \left| u_{ij}^2 \right| \quad (3)$$

Equations 2 and 3 are reduced to make the equations independent of the number of clusters (Garcia et al., 2017) where F_s is the normalized partitioning co-efficient and H_s is the normalized partitioning entropy.

$$F_s = \frac{F - \frac{1}{c}}{1 - \frac{1}{c}} \quad (4)$$

$$H_s = \frac{H - (1 - F)}{\ln(c) - (1 - F)} \quad (5)$$

2.3 Applying FCM to 3D datasets

Using the Scikit-Fuzzy package, a collection of fuzzy logic algorithms written in the Python computing language, the dataset X, where each element is classified by a density contrast, resistivity and velocity perturbation value [xi= (ρ_i, d_i,v_i)] were clustered into groups by utilizing the following steps:

1. Interpolate the datasets onto a common grid spacing. To ensure that all points are spatially coincident, the gravity and the resistivity models were downsampled to a grid spacing of 250 m. This was done with the use of a python script which utilized the basic interpolation function, nearest neighbour, of the python library SciPy. Hence any element within the dataset would now contain a respective density, velocity and resistivity value represented by [xi= (ρi, di,vi)].
2. Plot the spatial distribution of the velocity, density and resistivity on a 3D plot.
3. Determine the optimum number of clusters using the normalized partitioning coefficient and normalized entropy coefficient.
4. Complete the defuzzification process where each data point is assigned fully to the cluster to which it has highest membership.
5. Plot the spatial distribution of the clusters in Paraview.

3.0 RESULTS

3.1 Optimum number of clusters

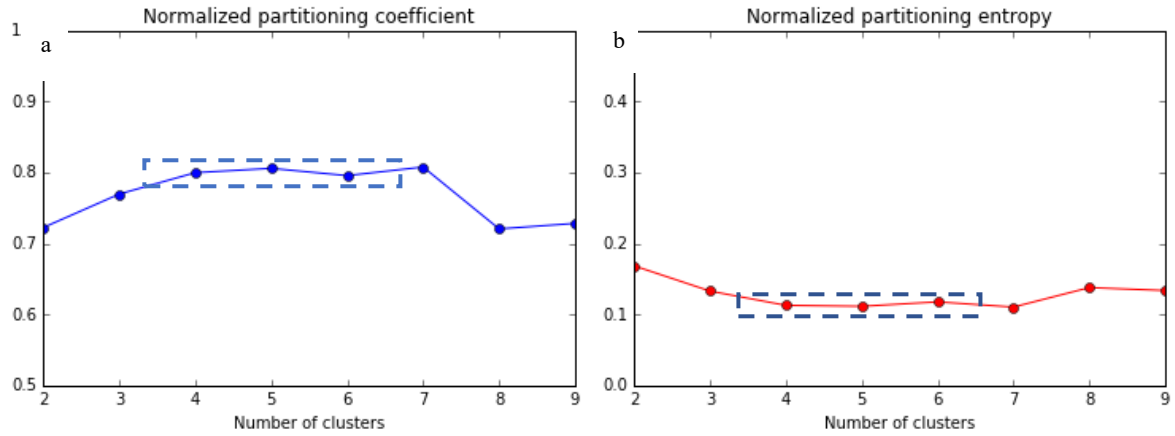

Figure 2 a) Variation of the Normalized partitioning coefficient from 2 to 9 clusters. b) Variation of the Normalized partitioning coefficient from 2 to 9 clusters.

Figure 2a and 2b which illustrate the variations in the normalized partitioning coefficient and the normalized partitioning entropy with clusters ranging from 2 to 9 are utilized to evaluate the optimum number of clusters for grouping the datasets. Both figures illustrate that clusters 4, 5, 6 and 7 have similar or little variation in normalized partitioning coefficient (NPC) and normalized entropy coefficient (NPE). To understand more about this, we compare the values of these validity indices to the values of the validity indices obtained by Garica et al (2017). In this study, both NPC and NPE vary by approximately 0.1. Garcia et al (2017) also obtained these approximate variations in both the NPC (0.45- 0.55) and NPE (0.3-0.4). We also utilize the 3D plot of density contrasts, Vp and log resistivity (Figure 3a) and investigate the variation in the membership values for these clusters to help determine the best number of clusters within the dataset. The clustering of the datapoints within the 3D plot appear to be arranged into either 3 or 4 distinct. Based also on the geological data available from MON-1 and MON-2 we utilize 4 clusters as the optimum choice to cluster the datasets.

3.1 Spatial distribution of clusters obtained from FCM

a

b

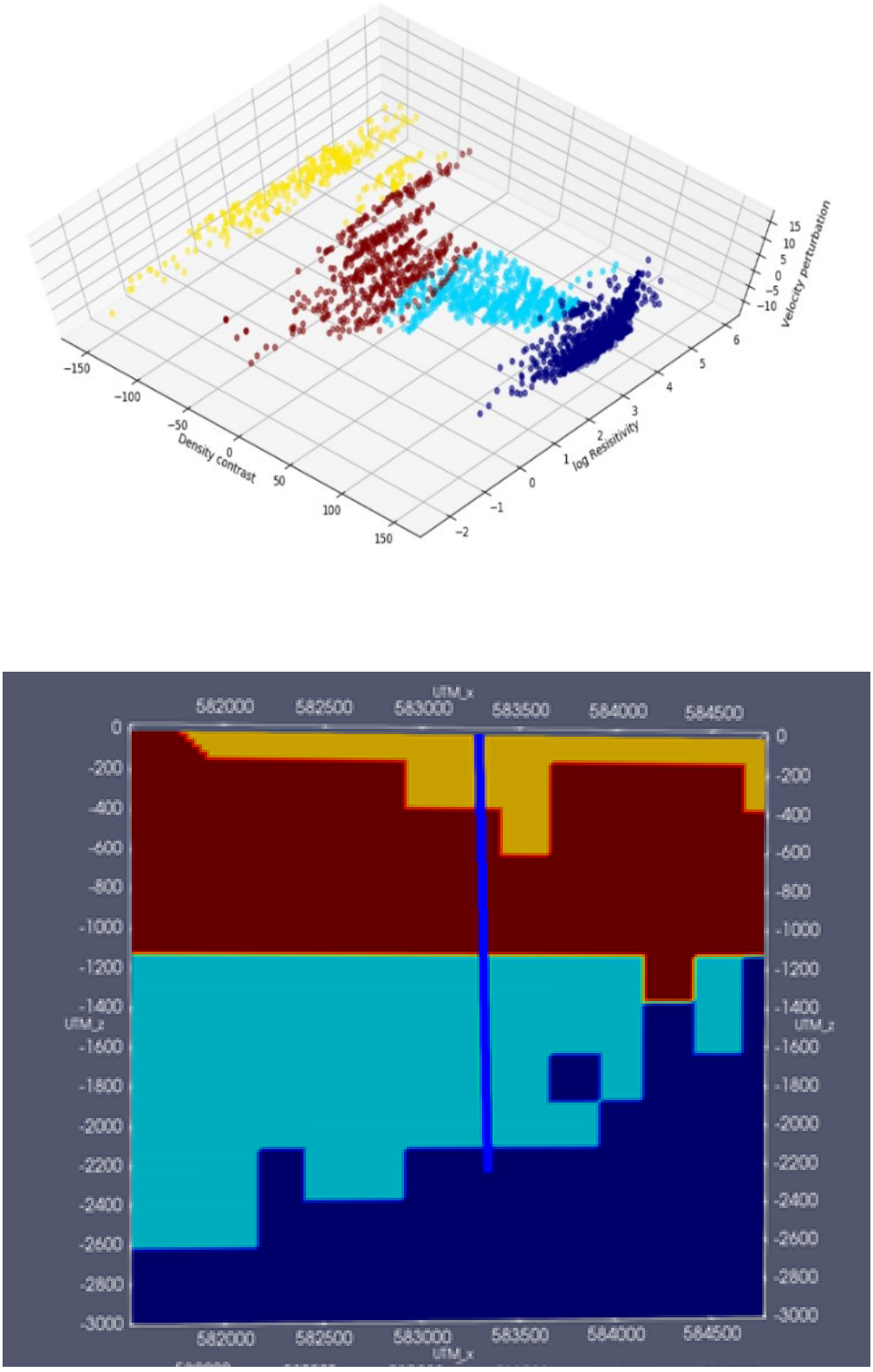

Figure 3a) A 3D plot highlighting the distribution of the four clusters obtained with the Fuzzy c means technique. b) A cross sectional slice through the FCM model at the location of MON-1 highlighting four main groups (cluster 1 yellow in colour from approximately 0- 300 mbsl, cluster 2 red in colour from 300 to 1200 mbsl, cluster 3 light blue in colour from 1200 to 2600mbsl and cluster 4, dark blue in colour and located to the north-eastern side of the cluster model.

3.2 Cluster Centers

Table 1: Four cluster centers were calculated from the fuzzy c means technique. Each cluster center is associated with a density contrasts (D_c), resistivity (R) and velocity perturbation (Vp) value.

Clusters	Dc (kg/m3)	R (Log_e Ohm.m)	Vp (%)	Joint geophysical parameters
1	-122.63	3.26	-1.00	Highest R, lowest D_c
2	-19.57	1.95	-1.23	Lowest R, med low D_c , low Vp
3	59.23	3.09	-4.94	Med R, med D_c, lowest Vp
4	142.34	3.11	-0.29	Highest D_c

4.0 DICUSSION

4.1 Cluster 1

Cluster 1 appears mainly from 0 to 300 mbsl (noted in Figure3 as the yellow structure). To interpret this feature of the Montserrat Geothermal system, the joint geophysical variations are utilized. Based on Table 1, cluster 1 most distinct geophysical feature are the lowest negative density contrasts (-122.63 kg/m^3) and the highest resistivity (3.26 log_e Ohm.m). To interpret these geophysical variations, we utilize table 1 which describes a list of geological materials logged at the locations of MON-1 and MON-2 (EGS, 2014). These geological materials were also reported in Harford et al (2002) and Rea (1974) who completed geological studies on Montserrat. Amongst these materials include andesite, the highest density, and volcanic breccia, clay and tuff of low densities. Assuming an average density of 2300 kg/m^3, lowest negative density contrasts (-233 kg/m^3 to -187 kg/m^3) are expected in the low density materials reported. While all three materials are possible interpretations for the lowest negative density contrasts observed, the highest resistivity variation obtained in cluster 1 is also used to constrain the interpretation of this cluster.

At depths 0 – 300 mbsl, which cluster 1 was obtained from the FCM analysis, temperatures between 30 - 40 °C are expected (based on temperature logs obtained from MON-1 and MON-2 (Ryan et al., 2014)). At these temperatures, rocks are reported as having little to no alteration (Flovenz et al., 1985). Clay minerals such as smectite are usually formed at temperatures at and greater than 40 °C (Flovenz et al., 1985; Frolova et al, 2014). In addition to this, smectite's high cation exchange capacity (80 -120 meq/100g) can result in low resistivities (Waxman and Smits (1968)) which was not described for this cluster. Hence, by utilizing the high resistivity obtained for cluster 1 we eliminate clay) as the possible interpretation of the cluster 1. Based on the joint analysis obtained from the cluster analysis we conclude that cluster 1's interpretation is consistent with unaltered volcanic breccia or tuff.

4.2 Cluster 2

Cluster 2 (noted in Figure 3 as the red structure) appears mainly from 300 mbsl to depths less than 1200 mbsl in the FCM model. The distinct geophysical parameters from the FCM model for cluster 2 are the medium low negative density contrasts (-19.57 kg/m^3) and the lowest resistivity (1.95 log_e Ohm.m).

Table 2: Average density and velocities obtained on geological materials reported in Montserrat and the gological materials obtained in Montserrat Geothermal wells (Tenzer et al., 2011)

Geological materials	Average Density (kg/m^3)	Average Velocity (km/s)
Andesite	2565	5.23
tuff	2113	1.43
Volcanic breccia	2195	4.22
Clay	2067	2.45
limestone	2484	4.80
sandstone	2463	2.80

In cluster 1's interpretation, low negative density contrasts were related to low density materials such as clays, volcanic breccia and tuff (Table 2). To differentiate between these materials for interpreting cluster 2, the resistivity variation is again utilized. Compared to cluster 1 (highest resistivity), cluster 2 has the lowest resistivity. Both Ussher et al (2000) and Waxmann and Smits (1968) note that the high cation exchange capacity (CEC) of clay minerals, in particular, smectite (CEC of 80 – 120 meq/100g) can result in low resistivities. However, in addition to smectite, there are two other minerals of low densities, that also can result in low resistivities. These two minerals, heulandite and stilbite are classed as zeolites (average density of 2200 and 2150 kg/m^3 respectively) (Bergaya et al., 2007). Zeolites may form where volcanic rocks, including ash layers, react with alkaline water via a

dissolution- re-precipitation process of amorphous alumino-silicate volcanic glass with pore water, or by the alteration of feldspars. Like smectites, zeolites are also characterized as having a high cation exchange capacity (CEC for heulandite was reported by Fridriksson et al (2004) as 300 meq/100g) which similarly can result lower resistivities (Frolova et al, 1985). We further utilize the velocity perturbation data to help interpret this cluster.

Schön (1998) reported that both heulandite and stilbite have velocities of 4.68 km/s and 4.48 km/s respectively while the velocity of smectite is 2.78 km/s. Investigating the velocity perturbation for cluster 2, this decreases to -1.23% within this cluster. Ryan et al (2014) hypothesized that the velocity perturbation anomaly was controlled to a first order by the degrees of hydrothermal alteration. More specifically, at temperatures between 50 to 90 °C, clays (smectite in abundance) are formed and acts to plasticize the rock matrix and reduce bulk and shear moduli of the rock which can result in reduced P-wave velocity. Since a reduction in the velocity occurs in cluster 2 (300 – 1200 mbsl), we eliminate zeolites as the possible interpretation for cluster 2. Auckland Uniservices Ltd (2016) also reported over 50 % of smectites (expressed as percentage of the total clays) at depths between 300 – 1200 mbsl in both MON-1 and MON-2.

In addition to the low temperature alteration minerals such as smectites, the presence of open fractured regions can also cause a reduction in the velocity. This however seems highly unlikely since this would imply that the density also decreases. In this cluster, density contrasts increases to a medium low (average -19.57 kg/m3 (table 1)). While confining pressure effects with depth can cause the density to increase with depth, the alteration of smectite to illite usually occurring at temperatures greater than 100 °C (Reyes, 2000) can also be a possible cause for the increase in density contrasts. Illite (average density of 2660 kg/m3) is another type of clay mineral that can possibly lead to increases in density. Based on the joint interpretation of all three geophysical properties obtained from the FCM cluster analysis we interpret cluster 2's interpretation is consistent with as the smectite/ smectite-illite clay cap.

4.3 Cluster 3

In comparison to cluster 1 and 2, cluster 3 has a medium positive density contrasts (59.23 kg/m3). Thus far, at temperatures between 50 to 90 °C, low alteration clays such as smectites are formed and are more prevalent (greater in quantity) compared to other clay minerals such as illite and chlorite. Illite and chlorite are formed at temperatures greater than 100 °C. Both high density minerals (2660 and 2800 kg/m3 respectively compared to smectite can be a possible cause for the increase in density (medium positive density contrasts) with depth. In addition to illite and chlorite, higher density minerals such as epidote and actinolite (3400 and 3040 kg/m3 respectively) are formed at temperatures greater than 200 °C (Reyes, 1967). Temperatures greater than 200 °C were measured at depths greater than 2000 mbsl at both MON-1 and MON-2 (EGS, 2016). While temperature increase with depth can result in high density alteration minerals and hence can lead to an increase in density contrasts, we also utilize the velocity perturbation and resistivity values obtained from the FCM to further constrain and justify the interpretation of cluster 3.

Cluster 3 has the lowest velocity perturbation (Table 1). A low velocity perturbation or slower than average velocities per depth can be interpreted as either high porosity rocks or fractured regions or alteration minerals of low velocities. However, the density contrasts obtained from the cluster analysis do not highlight this. Instead of a low density contrasts, a medium positive density contrasts was obtained in the cluster analysis for clusters 3. Further investigation into the velocity perturbation with depth shows that the lowest velocity perturbation is modelled to 1750 mbsl while at depths greater than 1750 mbsl it increases (Ryan et al., 2014). To describe this effect, Ryan et al (2014) postulated that the velocity anomaly observed within the Montserrat Geothermal project area (Figure 1) may be controlled to a first order by hydrothermal alteration. They noted that low temperature alteration minerals such as smectite causes the velocity to decrease while high temperature alteration minerals such as illite, chlorite, epidote and actinolite causes the velocity to increase.

To determine if these higher temperature alteration minerals usually formed within a geothermal reservoir can be a possible interpretation for cluster 3 we now investigate the resistivity variations. Illite and chlorite are characterized by lower cation exchange capacities (25 – 40 and 5 – 15 meq/100g) compared to smectites which can result in slightly higher resistivities (Ussher et al., 2000). From the cluster analysis, cluster 3 has a medium resistivity (3.09 $\log_e$ Ohm.m. Auckland Uniservices Ltd, (2016) also reported chlorite percentages between 40 to 80 % at MON-1 and 20 to 80 % at the location of MON-2 based on a clay analysis on drill cuttings obtained. The highest percentage were recorded at depths between 2000 to 3000 mbsl. They also reported approximately increasing illite percentages between 20 to 60 % for both wells. Utilizing variations in all three geophysical parameters, we interpret cluster 3 as the geothermal reservoir of the Montserrat geothermal system made up of higher alteration minerals.

4.4 Cluster 4

The spatial location of this cluster indicates that this region is located in the north-east of the MGS and at depths to 250 mbsl encircling the eastern side of Garibaldi hill. The distinct geophysical parameter of this cluster is that it has the highest positive density contrasts (average density contrasts of 142.34 kg/m^3). Table 1 describes the highest densities as andesite. Similarly, Hautmann et al (2013) reported that that the high density contrasts body located in the center of Montserrat or to the northeast of the MGS can be interpreted as the andesitic magmatic intrusions and remnants of feeder-systems form the cores of the extinct volcanic centre, Centre Hills. They also interpreted the high density body that appears at depths 0- 250 mbsl encircling the eastern side of Garibaldi Hill as bounding faults between Garibaldi Hill and St Georges Hill. To help better understand the high density body obtained at depths 250 mbsl with resistivity and velocity perturbation would be a challenge. This is because of the geophysical measurements for the magneteotellurics survey (resistivity data) were mainly constrained towards the south-western side of the island where the geothermal system is location. Hence the reliability of resistivity data within this region is questionable. In addition to this, the purpose of the gravity survey (density contrasts data) were to model the small seated anomalies that were not detected by the seismic tomography survey (velocity perturbation). We do however utilize the high velocity perturbations obtained with cluster 4 to interpret the high density body located to the north-east of the MGS to be consistent with the solidified magmatic intrusions of Centre Hills (also interpreted in Shalev et al., 2010).

CONCLUSION

The use of more than one geophysical parameter can be utilized beyond qualitative correlations to help constrain the interpretation of the Montserrat Geothermal system. The similarities of three 3D geophysical datasets, velocity perturbation, resistivity and density contrasts, were investigated with the use of a machine learning technique: The Fuzzy c- means. The joint interpretation allowed for the similar groups to be constrained with different geophysical parameters. Variations within each group or class were used to identify the main structural feature of the MGS. Cluster 1 was interpreted as an unaltered region, Cluster 2 was interpreted as the smectite/ smectite-illite clay cap, cluster 3 was interpreted as the geothermal reservoir comprised of higher temperature alteration minerals and cluster 4 was interpreted as an intrusion. Further work involves investigating the stability of this cluster analysis and mapping the regions of low resolution within each geophysical geophysical dataset. Additionally, more work will be focused on investigating the correlations between the geophysical parameters obtained from this cluster analysis and direct measurements made on core samples obtained from a third geothermal well drilled in Montserrat. The advantage of the cluster analysis is that each structure is now assigned more than one geophysical parameter that can be used to refine previous calculations on petrophysical parameters, such as saturation, permeability and porosity by utilizing existing rock physics models. Future work involves combining this model with laboratory petrophysical measurements on cores obtained from the third well drilled in Montserrat.

REFERENCES

Auckland Uniservices Ltd.: Advanced Petrological study of the Montserrat Geothermal Project area. (2016)

F. Bergaya, B.K.G. Theng & G. Lagaly.: Handbook of Clay Science. Developments in Clay Science, 1. Elsevier Ltd. (2007)

Bezdek, J. C., R. Ehrlich, and W. Full.: FCM: The fuzzy c-means clustering algorithm: Computers and Geosciences, 10, . (1984)191– 203, doi: 10.1016/0098-3004(84)90020-7

Brophy, P., Poux, B., Suemnicht, G., Hirtz, P., & Ryan, G.: Preliminary results of deep geothermal drilling and testing on the island of Montserrat. *Proceedings* of the Thirty-Ninth Workshop on Geothermal Reservoir Engineering, Stanford, CA, USA (2014).

De Stefano, M., F. G. Andreasi, S. Re, and M. Virgilio.: Multipledomain, simultaneous joint inversion of geophysical data with application to subsalt imaging: Geophysics, **76**, (2011) no. 3, R69–R80, doi: 10.1190/1.3554652.

EGS Inc, Final Report Geothermal Exploration in Montserrat Caribbean, (2010)

Flóvenz, Ó.G., Hersir, G.P., Sæmundsson, K., Ármannsson, H., and Friðriksson,.: Geothermal Energy Exploration techniques. In Sayigh, A. (ed.) Comprehensive Renewable Energy, Oxford: Elsevier. 7, 51–95 2012.

Franzson H., Zierenberg, R., Schiffman, P.: Chemical transport in geothermal systems in Iceland evidence from hydrothermal alteration. Journal of Volcanology and Geothermal Research, **173** (2012) 217–229.

Frolova, J, Gvozdeva. I, Kuznetsov, N.: Effects of Hydrothermal alteration on physical and mechanical properties of rocks in geysers valley (Kamchatka Peninsula) in Connection with Landslide Development. *Proceedings* World Geothermal Congress, (2015).

Fridriksson, Th., Neuhoff, P.S., Vinani, B.E., and Bird, D.K.: Experimental determination of thermodynamic properties of ion-exchange in heulandite: binary ion-exchange experiments at 55 and 85°c involving Ca2+, Sr2+, Na+ and K+. American Journal of Sciences **304**, (2004), 287–332.

García-Yeguas, A., J. Ledo, P. Piña-Varas, J. Prudencio, P. Queralt, A. Marcuello, J. M. Ibañez, B. Benjumea, A. Sánchez-Alzola aand N. Pérez.: A 3D joint interpretation of magnetotelluric and seismic tomographic models: The case of the volcanic of Tenerife, Computers & Geosciences 109: 95-105, (2017

Gallardo, L. A., and M. A. Meju.: Joint two-dimensional DC resistivity and seismic travel time inversion with cross-gradients constraints: Journal of Geophysical Research (Space Physics), 109, (2004)

Hatter, J.: The long term evolution of Montserrat Volcanism, Ph.D dissertation University of Southampton, (2018)

Harford, C.L., Pringle, M.S., Sparks, R.S.J., Young, S.R., 2002.: The volcanic evolution of Montserrat using 40Ar/39Ar geochronology. Geol. Soc. London, Mem. 21, (2002), 93–113

Hautmann, S., Camacho, A.G., Gottsmann, J., Odbert, H.M., Syers, R.T.: The shallow structure beneath Montserrat (West Indies) from new Bouguer gravity data. Geophys. Res. Lett. 40, (2013) 5113–5118. doi:10.1002/grl.51003.

Paasche, H., and J. Tronicke.: Cooperative inversion of 2D geophysical data sets: A zonal approach based on fuzzy c-means cluster analysis: Geophysics, **72**, no. 3, (2007) A35–A39, doi: 10.1190/1.2670341.

Paasche, H., J. Tronicke, and P. Dietrich.: Automated integration of partially co-located models: Subsurface zonation using a modified fuzzy c-means cluster analysis algorithm: Geophysics, 75, no. 3, (2010), 11–22, 10 .1190/1.3374411.

Rea, W.J.: The volcanic geology and petrology of Montserrat, West Indies. J. Geol. Soc. London. 130, (19)74341–366.

Reyes, A.: Petrology and mineral alteration in hydrothermal systems: From diagenesis to volcanic catastrophes, United Nations University Training Programme 1998 -Report **18**, (2010)

Ryan, G. A., and E. Shalev.: Seismic Velocity/Temperature Correlations and a Possible New Geothermometer: Insights from exploration of a High-Temperature Geothermal System on Montserrat, West Indies. Energies 7 (10), (2014), 6689-6720.

Ryan, G. A., J. R. Peacock, E. Shalev, and J. Rugis.: Montserrat geothermal system: A 3D conceptual model, Geophys. Res. Lett., 40, (2013)

Ryan, G. A., S. A. Onacha, E. Shalev, and P. E. Malin.: Imaging the Montserrat geothermal prospect using Magnetotelluric (MT) and Time Domain Electromagnetic induction (TDEM) measurements, Auckland, New Zealand: Institute of Earth Science and Engineering, (2009).

Schön, J. H.: Physical properties of rocks: Fundamentals and principles of petrophysics: Pergamon Press, Inc. 1998.

Sun, J., and Y. Li.: Joint inversion of multiple geophysical data: A petrophysical approach using guided fuzzy c-means clustering: 82nd Annual International Meeting, SEG, Expanded Abstracts,1–5, (2012)

Tenzer, R., Sirguey, P., Rattenbury, M., and Nicolson, J. A digital rock density map of New Zealand, Computers & Geosciences. **37**, (2011), 1181-1191.

Ussher, G.; Harvey, C.; Johnstone, R.; Anderson, E.: Understanding the resistivities observed in geothermal systems. *Proceedings* of the World Geothermal Congress, Kyushu-Tohuku, Japan, (2000)

Waxman, M.H. and Smits, J.M.: Electrical conductivities in oil-bearing shaley sands: Soc. Pet. Eng, (1968)